Freezing transition and correlated motion in a quasi-two-dimensional colloid suspension

Ronen Zangi
Department of Biophysical Chemistry, University of Groningen, Nijenborgh 4, 9747 AG Groningen, The Netherlands

Stuart A. Rice
Department of Chemistry and The James Franck Institute, The University of Chicago, Chicago, Illinois 60637, USA

(Received 12 June 2003; published 24 December 2003)

Recent experiments have demonstrated that the deviation of the single-particle displacement distribution from Gaussian form in a dense quasi-two-dimensional colloid suspension is a result of heterogenous dynamics that involves cooperative motions of neighboring colloid particles [J. Chem. Phys. **47**, 9142 (2001)]. In this paper, we report the results of molecular dynamics (MD) simulations of a quasi-two-dimensional assembly of nearly hard-sphere colloid particles. The colloid-colloid interaction we use is short ranged and everywhere repulsive; it is related to the Marcus-Rice (MR) and modified MR interactions used in a previous study [Phys. Rev. E **58**, 7529 (1998)]. As is the case for those systems, the one we study supports liquid, hexatic, and solid phases. Our calculations show that the deviation of the single-particle displacement distribution from Gaussian form is present in the liquid phase, and that a sharp increase in its magnitude occurs at the liquidus density and extends into the crystalline phase. For densities greater than the liquidus density we find three dynamical relaxation processes that include, at intermediate times, a slowing down in the rate of growth of the diffusive displacement of a particle due to the cage effect. As the density increases toward the solidus density, the dependence of the mean squared displacement on time, at intermediate times, changes from sublinear to zero. The onset of the long-time relaxation mode corresponds to the time at which the deviation of the particle displacement distribution from Gaussian form is a maximum. At this time, which increases exponentially with the density, the self-part of the van Hove function exhibits multiple maxima with respect to r while the distinct part of the van Hove function is a maximum at the origin, thereby signaling jump dynamics. At long times the particle mean square displacement has diffusive character at all densities including solid phase densities. A remarkable feature of our findings is the continuity of character of the particle displacement from the liquid phase through the hexatic phase and into the solid phase. Cooperative jumps that lead to diffusive process in crystals can be explained by a mechanism that involves many such correlated hops in random locations and random directions (but along the crystallographic axes) thereby generating effective random walk behavior. We argue that the collective motion we have found is generated by superpositions of instantaneous normal mode vibrations along diffusive paths. The diffusive paths are along the directions with strong bond orientation correlation, and start to grow in amplitude rapidly on entry into the hexatic phase.

DOI: 10.1103/PhysRevE.68.061508 PACS number(s): 64.70.Dv, 82.70.Dd

I. INTRODUCTION

The character of one-particle motion in a medium can be used to monitor the contributions of cooperative effects to the particle displacement dynamics. In an ideal gas the displacement of a particle is independent of the displacements of the other particles. Then the probability that a particle will move a distance r in time t, $G_s(r,t)$, is proportional to the probability of its having a velocity with the magnitude r/t as given by the Maxwell-Boltzmann distribution. The probability distribution $G_s(r,t)$ known as the self-part of the van Hove function is, therefore, proportional to $e^{-mr^2/2k_BTt^2}$. This free-particle behavior is applicable to all media at all densities in the limit $t\rightarrow 0$. In the hydrodynamic limit, $t\rightarrow\infty$, when cooperative effects dominate the particle displacement in a dense liquid, the solution of the diffusion equation also yields a Gaussian form for $G_s(r,t)$ [1]. In both limits, $G_s(r,t)$ in two dimensions can be written as

$$G_s(r,t)=\frac{\alpha(t)}{\pi}e^{-\alpha(t)r^2}, \tag{1}$$

where $\alpha(t)$ is obtained by expressing the mean squared displacement $\langle r^2(t)\rangle$ as a spatial integral of $G_s(r,t)$. Then $\alpha(t)=1/\langle r^2(t)\rangle$. If $G_s(r,t)$ has a Gaussian form the averages of the even-power moments of the single particle displacement distribution satisfy the following relation:

$$\langle r^{2n}(t)\rangle = n!\langle r^2(t)\rangle^n. \tag{2}$$

Therefore, deviations from the Gaussian approximation can be measured by a time-dependent term $\alpha_n(t)$

$$\alpha_n(t)=\frac{\langle r^{2n(t)}\rangle}{n!\langle r^2(t)\rangle^n}-1. \tag{3}$$

Deviations from the Gaussian distribution of particle displacements that occur in the intermediate time regime in three-dimensional systems are very small [2–4]. In these cases the first correction to the Gaussian approximation is typically 10% or less of the leading term and successive terms are even smaller. Stronger deviations from Gaussian behavior has been observed in dense glass-forming liquids just above the glass transition [5–8].

Recently, it has been shown, both computationally [9–12] and experimentally [13,14], that the motion of dense two-dimensional liquids is heterogenous and the single-particle displacement distribution has a very large non-Gaussian component. Moreover, it is found that in these dense liquids the single-particle displacement involves cooperative stringlike motions in some time regimes.

Consider the case of a simple fluid. For times shorter than the average collision time the particle motion is ballistic, hence the mean squared displacement is a quadratic function of time. At long times, the stochastic nature of successive interactions with the neighboring particles generates dynamics that can be represented by a Brownian motion model. In this regime the mean squared displacement of a particle is a linear function of time. In three dimensions the interpolation between these two time regimes extends over a short time period and the deviations from Gaussian behavior are very small; these deviations can be accounted for by memory function analysis of the autocorrelation function of the random force. However, in a high density two-dimensional liquid the asymptotic diffusive behavior is reached very slowly. The large magnitude deviations from Gaussian behavior in the intermediate-time regime suggest that the mechanism of the one-particle motion of the particles is different; the lack of vacancies in the first-neighbor shell surrounding a molecule (''cage effect'') inhibits large displacements and local rearrangements can only occur through the correlated motion of many particles along pathways that preserve the local continuity of the system. Such local rearrangements typically occur in domains which are temporarily more ''fluidized'' than the background.

The notion of correlated motion in so-called ''cooperatively rearranging regions'' was first introduced by Adam and Gibbs for the case of dense glass-forming liquids [15]. The typical size of these cooperatively rearranging regions is postulated to grow with decreasing temperature.

Marcus, Schofield, and Rice [13] reported the results of experimental studies that show the presence of stringlike cooperative motions in a dense quasi-two-dimensional liquid. They observed that the self-part of the van Hove function developed a second peak due to an activated process in which a particle hops to one of the positions that was formerly occupied by one of the cage particles that initially surrounded it.

Further studies by Cui, Lin, and Rice [14] found that the one-particle displacement dynamics can be described in terms of three relaxation processes; the contributions of these processes to the particle mean squared displacement vary with time so that one or the other is dominant in different time domains. In particular, they found that at intermediate times the mean squared displacement has a sublinear dependence on time, while, at long times there is an increase in the mean squared displacement due to contributions from infrequent large displacements, of the order of a particle diameter in length. The spatial configurations of the particles consisted of dynamically ordered domains separated by fluidized boundaries. The displacement of a particle in the fluidized boundary region was correlated with the displacement of its neighbors. As a consequence, the time dependence of the particle displacement at intermediate times had mixed character due to contributions from several different kinds of motions.

In three-dimensional systems, deviations of the mean squared displacement of a particle from Gaussian behavior have been reported from the results of experiments performed on bulk colloidal suspensions [7,8] and on supercooled orthoterphenyl [16]. Such deviations have also been reported from the results of simulations of the hard-sphere liquid [17], Lennard-Jones binary mixtures [5,6,18,19], and polymer melts [20–22]. In all of the cases cited the findings are interpreted in terms of the transition to the glass state. However, in the quasi-two-dimensional systems mentioned above, the dense colloidal suspensions do not exhibit a glass transition; rather, they freeze to form a hexagonal crystalline phase.

Mode-coupling theory predicts that three-dimensional dense liquids near the glass transition exhibit a distinct separation of relaxation time scales, specifically a slow global relaxation identified as the α-relaxation process and an intermediate rate relaxation identified as the β-relaxation process [23–25]. A theoretical analysis that incorporates the effects of both mode coupling and binary uncorrelated collisions on the memory function has been used to describe the dynamics of quasi-two-dimensional confined colloid suspensions [26].

Diffusion in a crystal is normally accounted for by the motion of defects. For systems of the type we consider the most important defect is a lattice vacancy. Almost all extant theories of diffusion in a crystal use the assumption that atom jumps into vacancies are independent of one another, hence generate a random walk [27]. In general, if the defects are randomly distributed then the assumption that the motions of the migrating particles are independent leads to a Gaussian distribution of one-particle displacements at long time. Rice and co-workers showed that the one-particle diffusion coefficient can be represented in terms of a superposition of the normal vibrations of the crystal that have nonvanishing projections on the path between an occupied site and a neighboring vacant site [28–32]. Two-dimensional solids are qualitatively different from three-dimensional solids. In the former case, translational correlations are destroyed as $r \rightarrow \infty$ by long wavelength thermal fluctuations [33–36]. The unusual character of the melting transition in two-dimensional solids is described by the well known Kosterlitz–Thouless–Halperin–Nelson–Young (KTHNY) theory [37–41]. This theory predicts that the two-dimensional solid melts via a two stage process: first a continuous transition to a hexatic state, followed by a continuous transition to the liquid state. Zippelius has argued further that due to the nonlinearity of the hydrodynamic equations in two dimensions, the damping rates of phonon excitations in two-dimensional solids diverge logarithmically [42]. Taken together, all of these peculiarities of two-dimensional solids suggest that the diffusion mechanism might also differ from its three-dimensional counterpart.

In this paper, we present the results of extensive simulations of a quasi-two-dimensional colloid assembly. Our calculations show that the deviation of the single-particle displacement distribution from Gaussian form is present in the

liquid phase, and that a sharp increase in its magnitude occurs at the liquidus density and extends into the crystalline phase. For densities greater than the liquidus density we find three dynamical relaxation processes that include, at intermediate times, a slowing down in the rate of growth of the diffusive displacement of a particle due to the cage effect. As the density increases toward the solidus density, the dependence of the mean squared displacement on time, at intermediate times, changes from sublinear to zero. The onset of the long-time relaxation mode corresponds to the time at which the deviation of the particle displacement distribution from Gaussian form is a maximum. At this time, which increases exponentially with the density, the self-part of the van Hove function exhibits multiple maxima with respect to r while the distinct part of the van Hove function is a maximum at the origin, thereby signaling jump dynamics. At long times the particle mean square displacement has diffusive character at all densities including solid phase densities. A remarkable feature of our findings is the continuity of character of the particle displacement from the liquid phase through the hexatic phase and into the solid phase. Cooperative jumps that lead to diffusive process in crystals can be explained by a mechanism that involves many such correlated hops in random locations and random directions (but along the crystallographic axes) thereby generating effective random walk behavior. We argue that the collective motion we have found is generated by superpositions of instantaneous normal mode vibrations along diffusive paths. The diffusive paths are along the directions with strong bond orientation correlation, and start to grow in amplitude rapidly on entry into the hexatic phase.

II. METHODS

The model systems that we study consist of a single layer, with $N=2016$ particles, placed in a quasi-two-dimensional simulation box. The simulation box is rectangular in the xy plane, with side lengths in the ratio $x/y=7/(8\sqrt{3}/2)$; it has a height slightly greater than the particle diameter (see below). Periodic boundary conditions were imposed in the x and y directions, but not in the z direction. The calculations were carried out, and the results are reported below, in terms of the reduced variables $r^*=r/\sigma$, $z^*=z/\sigma$, $T^*=k_BT/\varepsilon$, $\rho^*=\rho\sigma^2$, $t^*=t(k_BT/m\sigma^2)^{1/2}$, $m=1$, with σ the diameter of the particle, ρ the number density, m the mass of the particle, t the time and 3.689ε is the value of the interparticle potential at $r^*=1.000$. Although the particles can move in the z direction under the influence of a z-dependent one-body potential, we choose to characterize the state of the system with the two-dimensional number density $\rho=N/A$, where A is the area of the simulation cell in the xy plane, since the height of the cell H is constant in all of the simulations presented in this paper. The same number of particles was present in the simulation cell for all of the densities studied. To study the properties of the system with different particle densities we changed the area of the simulation cell in the xy plane.

The interparticle potential was represented by

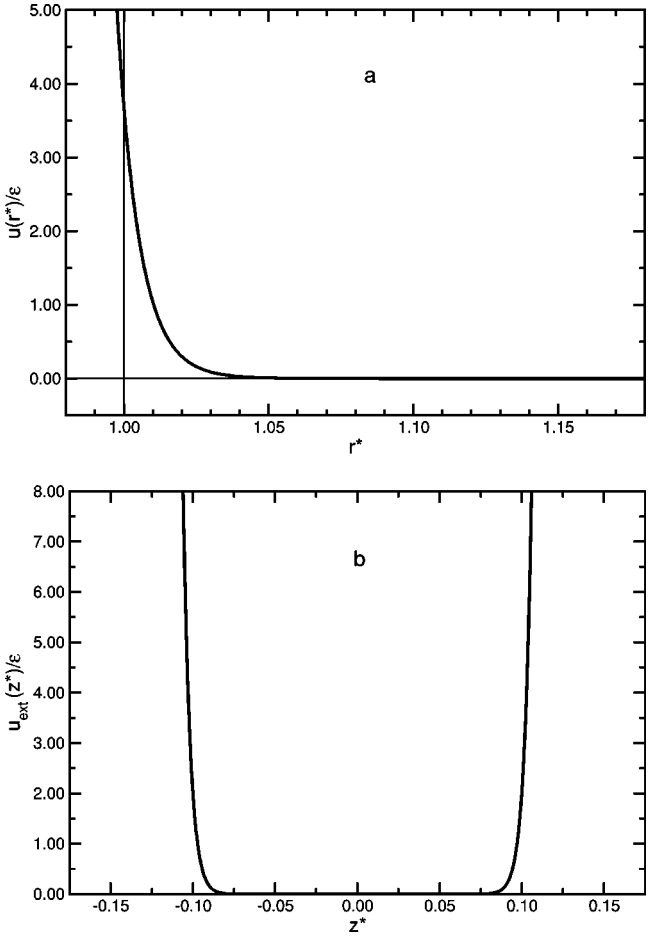

FIG. 1. (a) The interparticle potential between colloid particles used in this study. (b) The external potential confining the particles to a slab with height of $H=1.20\sigma$. The external potential is plotted as a function of the reduced center of mass coordinate along the vertical axis (z axis) measured from the center of the cell.

$$u(r^*)=A\left(r^*-\frac{1}{2}\right)^{-\alpha} \tag{4}$$

with $A=2\times10^{-19}$ and $\alpha=64$. The functional form in Eq. (4) is very nearly a hard-core repulsion but has continuous derivatives. It is plotted in Fig. 1(a). We note that the potential represented in Eq. (4) differs from the potential we used previously to study the equilibrium properties of a quasi-two-dimensional colloid system by omission of two terms in that potential; a narrow attractive well centered at $r^*=1.05$ and an interpolating soft repulsion.

The confinement of the particles in the $\pm z$ directions is affected by the action of a one-body z-dependent external field. Different forms can be chosen for this field, the simplest being that for hard parallel walls. Then the extra degree of freedom that is introduced in the thermodynamic description of the system is the spacing between those two walls. Because of their macroscopic size, colloidal spheres do not ''feel'' the atomic scale granularity of the walls, so the walls can be regarded as smooth. The shape of the potential that was chosen,

$$u_{\mathrm{ext}}(z^*) = D\varepsilon(z^*)^{\zeta}, \tag{5}$$

is such as to confine the system to form a slab with well specified height H. In Eq. (5) z^* is the distance from the center of the cell to the center of mass of the particle and $\zeta = 24$, $D = 2\times 10^{24}$; this potential confines the particles as if they were in a cell with an effective height of $H = 1.20\sigma$ (i.e., $z^* = \pm 0.10$) and is shown in Fig. 1(b).

The MD simulations were carried out in the microcanonical ensemble using the ''velocity Verlet'' algorithm [43,44]. The distance at which the potential was cut off was 1.5σ and the time step used was, in reduced units, 5×10^{-4}; the associated r.m.s. fluctuation in total energy did not exceed one part in 10^5.

The initial configurations for the simulations were taken from previous simulations that studied the thermodynamic behavior of a similar system with the Marcus-Rice interparticle potential [45]. At each density the required temperature was created in a preequilibration stage by multiplying the velocities, every 1×10^5 MD steps, by an appropriate constant. This stage was repeated until the difference between the average temperature of the system and the prescribed temperature $T^* = 1.0000$, did not exceed 5×10^{-4} in reduced units. Then the system was further equilibrated for 7×10^6 MD steps, and thermodynamics data collected for additional 5×10^6 MD steps, every 1000 time steps. The simulations studied 19 densities in the range $0.740 \leqslant \rho^* \leqslant 0.980$ that covers the transition from the liquid phase to the solid phase.

The investigation of the time-dependent properties of the system was performed separately after the thermodynamic data collection stage. To allow for effects associated with the very great difference in magnitude of the different dynamic relaxation times, at each density we carried out 3–5 simulations that extended for different lengths of time and used different time intervals for construction of the correlation functions. The time intervals covered by the different simulations overlapped in some regions. We checked the convergence of the results by requiring that the values of the computed dynamical properties in these overlapped time regions are the same in the different simulations.

The equilibration and the two data collection stages (dynamics and thermodynamics) were carried out without velocity rescaling (thus, in the microcanonical ensemble) to ensure uninterrupted dynamical paths. Nevertheless, the r.m.s. deviation of the average temperature from $T^* = 1.0000$ was less than 5×10^{-4}.

The lateral pressure P_l was calculated from

$$P_l = \frac{Nk_BT + \langle \mathcal{W}_l \rangle}{V}, \tag{6}$$

where the angular brackets indicate an average value, the volume V is $V = AH$ and the lateral virial $\mathcal{W}_l$ is

$$\mathcal{W}_l = -\frac{1}{2}\sum_{i=1}^{N}\sum_{j>i}^{N} \frac{x_{ij}^2 + y_{ij}^2}{r_{ij}} \frac{\partial u(r)}{\partial r}\bigg|_{r=r_{ij}}. \tag{7}$$

The structural properties of the system were characterized by calculating the radial distribution function $g(r_{xy})$

$$g(r_{xy}) = \frac{A}{2\pi r_{xy} N(N-1)} \left\langle \sum_{i=1}^{N}\sum_{j\neq i}^{N} \delta(r_{xy} - |\mathbf{r}_{xy,i} - \mathbf{r}_{xy,j}|) \right\rangle, \tag{8}$$

where $\mathbf{r}_{xy}$ is the lateral vector component of the particle's position, and the bond-orientation function $G_6(r_{xy})$,

$$G_6(r_{xy}) = \langle \Psi_6^*(0)\Psi_6(r_{xy}) \rangle, \tag{9}$$

where $\Psi_6(r_{xy})$ is the local order parameter descriptive of the hexagonal symmetry characteristic of close packing in two dimensions; it is defined by

$$\Psi_{6i} = \frac{1}{n_i}\sum_{j=1}^{n_i} e^{i6\theta_{ij}}. \tag{10}$$

The sum in Eq. (10) is taken over the n_i nearest neighbors to particle i, as determined by a two-dimensional Voronoi polygon construction [46]. We denote by θ_{ij} the angle between the vector $\mathbf{r}_{xy,ij}$ and an arbitrary fixed axis. The global translational order parameter is defined to be the sum of the Fourier components of the density

$$\Phi_T = \frac{1}{N}\sum_{i=1}^{N} e^{i\vec{G}\cdot\vec{r}_i}, \tag{11}$$

where $\vec{G}$ is a reciprocal lattice vector of the triangular two-dimensional lattice. The corresponding global orientational order parameter is defined by

$$\Phi_6 = \frac{1}{N}\sum_{i=1}^{N} \Psi_{6i}. \tag{12}$$

The lateral mean square displacement $\Delta r_{xy}^2(t)$ was calculated using the following expression:

$$\langle \Delta r_{xy}^2(t) \rangle = \frac{1}{N}\sum_{i=1}^{N} [\mathbf{r}_{xy}(t) - \mathbf{r}_{xy}(0)]^2. \tag{13}$$

We describe the time-dependent deviation of the particle displacement from Gaussian behavior by the non-Gaussian parameter $\alpha_2(t)$. In two dimensions it has the following representation:

$$\alpha_2(t) = \frac{\langle [\mathbf{r}_{xy}(t) - \mathbf{r}_{xy}(0)]^4 \rangle}{2\langle [\mathbf{r}_{xy}(t) - \mathbf{r}_{xy}(0)]^2 \rangle^2} - 1. \tag{14}$$

In order to provide a measure for the deviation from Gaussian behavior over all times we integrate the absolute value of $\alpha_2(t)$ over time in the following way:

$$I\{|\alpha_2[\ln(t)]|\} = \int |\alpha_2[\ln(t)]| d\ln(t). \tag{15}$$

The normalized velocity-velocity autocorrelation function was calculated from

$$C_{vv}(t)=\frac{\langle \mathbf{v}_{xy}(0)\cdot\mathbf{v}_{xy}(t)\rangle}{\mathbf{v}_{xy}(0)\cdot\mathbf{v}_{xy}(0)}, \tag{16}$$

where $\mathbf{v}_{xy}$ is the lateral vector component of the particle's velocity.

Time-dependent spatial correlations of the particles positions were examined using the van Hove function [47]. It is convenient to represent the "self" part $G_s(r_{xy},t)$ and the "distinct" part $G_d(r_{xy},t)$ of the van Hove function separately. The self-part of the van Hove function, is the probability of finding a particle at time t and at distance r_{xy} given that at $t=0$ it was at the origin. It is defined by

$$G_s(r_{xy},t)=\frac{1}{2\pi r_{xy}N}\left\langle \sum_{i=1}^{N}\delta(r_{xy}-|\mathbf{r}_{xy,i}(0)-\mathbf{r}_{xy,i}(t)|)\right\rangle. \tag{17}$$

The distinct-part of the van Hove function is the probability of finding a particle j, $j\neq i$, at time t and at distance r_{xy} given that at $t=0$ particle i was at the origin. It is defined by

$$G_d(r_{xy},t)=\frac{1}{2\pi r_{xy}N}\times\left\langle \sum_{i=1}^{N}\sum_{j\neq i}^{N}\delta(r_{xy}-|\mathbf{r}_{xy,i}(0)-\mathbf{r}_{xy,j}(t)|)\right\rangle. \tag{18}$$

Thus, $G_d(r_{xy},0)=\rho g(r_{xy})$. For all calculations of the time-dependent properties of the system care was taken to assure that the analysis did not cover times for which the displacements of the particles exceeded half of the box length in the x or y direction.

III. RESULTS

Figure 2(a) displays the lateral pressure as a function of the two-dimensional number density in the range $0.740\leqslant\rho^*\leqslant0.980$ for the colloid-colloid potential used in this study. The lateral-pressure-density isotherm exhibits a plateau region (or a weak van der Waals loop) in the density range $0.865\leqslant\rho^*\leqslant0.895$ indicating a first-order phase transition. Figure 2(b) displays the global translational and orientation order parameters as a function of density. For densities $\rho^*\leqslant0.860$ the system is in the liquid phase, for densities $0.870\leqslant\rho^*\leqslant0.890$ it is in the hexatic phase, while for densities $\rho^*\geqslant0.900$ the system is in the solid phase. Despite the occurrence of a plateau in the isotherm coexisting phases were not found in this region. We believe the absence of coexisting phases in our simulation sample is a consequence of the finite size of the system, the small density range over which the hexatic phase is stable, and the form of the colloid-colloid interaction.

The radial distribution function and the bond-orientation correlation function are plotted in Fig. 3 for $\rho^*=0.860$, 0.880, and 0.900. Both correlation functions have short-range order for the liquid phase and long-range order for the solid phase, while the bond order correlation is long ranged and the pair correlation function is short ranged in the hexatic phase. The equilibrium properties of this system are

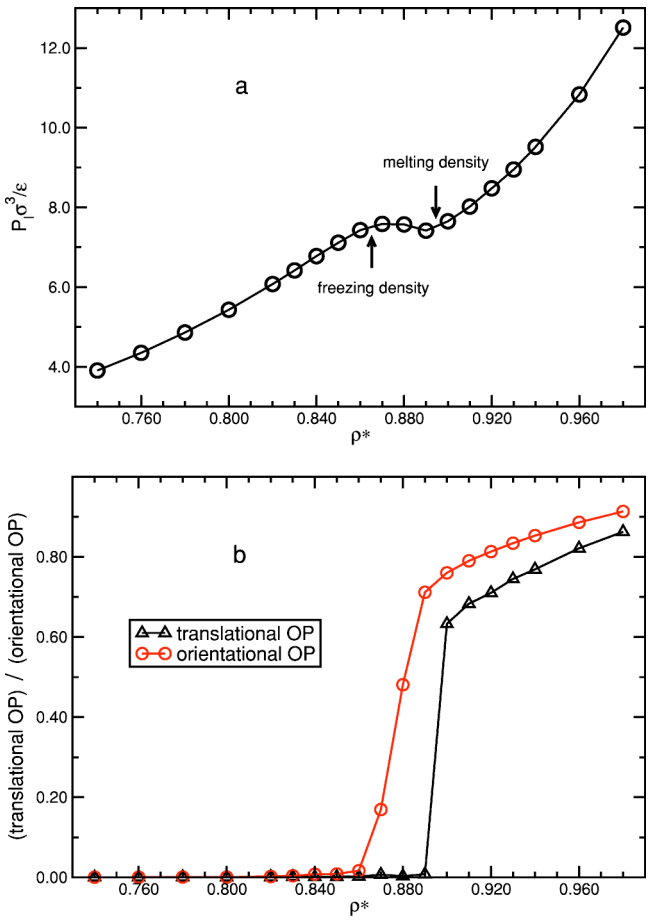

FIG. 2. (Color online) (a) The lateral pressure (in reduced units) as a function of the two-dimensional number density. The low-density end of the plateau region at $\rho^*=0.865$ signifies the onset of the liquid phase while the high-density end at $\rho^*=0.895$ marks the onset of the solid phase. (b) The global translational and orientation order parameters indicating that the hexatic phase is stable for $0.870\leqslant\rho\leqslant0.890$.

very similar to those found in our earlier study using the MR and modified MR colloid-colloid interaction [45,48]. They differ somewhat from those obtained experimentally by Karnchanaphanurach, Lin, and Rice for a quasi-two-dimensional suspension of silica spheres in water confined in a very thin glass cell [49]. The colloid-colloid interaction in that system is believed to be extremely short ranged, much closer to a hard-sphere interaction than the interactions used in this paper and our previous paper.

As a measure of the magnitude of the deviation from Gaussian form of the particle displacement distribution we plot in Fig. 4 the integral of the non-Gaussian parameter, defined in Eq. (15), as a function of the two-dimensional number density. Although the value of the integral is very small for the liquid phase, the particle motion is clearly heterogeneous and correlated motion can be observed (see below). However, at $\rho^*=0.870$, there is a sharp increase in the value of the integral indicating an increasing deviation from the Gaussian displacement distribution as the hexatic phase forms. The growing deviation from a Gaussian displacement distribution extends into the solid phase. Due to the exponen-

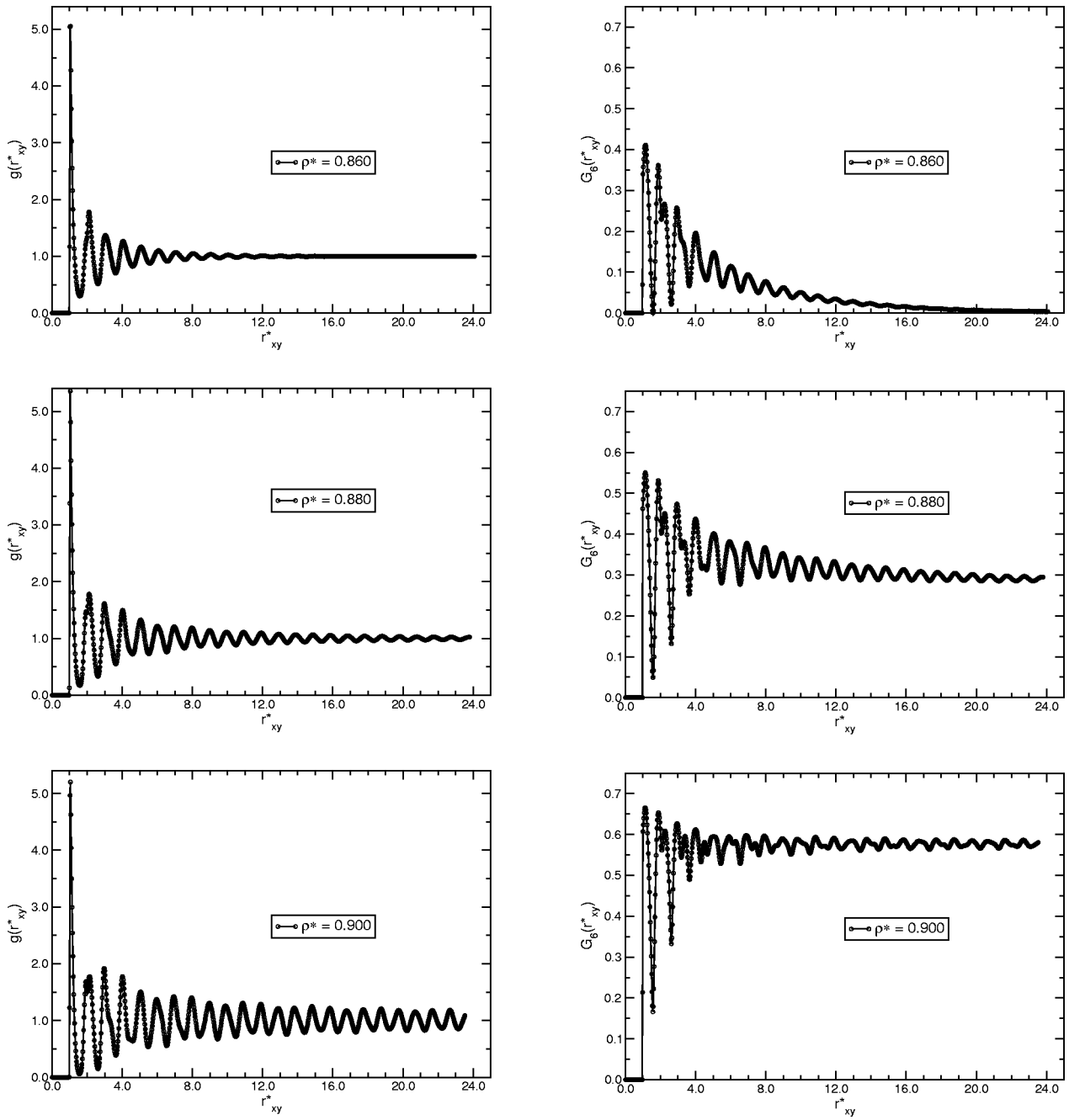

FIG. 3. The pair distribution function $g(r_{xy})$ (left panel) and the bond-orientation function $G_6(r_{xy})$ (right panel) for $\rho^*=0.860$, 0.880, and 0.900 displaying the characteristic structural properties of the liquid, hexatic, and solid phases, respectively.

tial increase in magnitude of the relevant dynamical relaxation times, we are unable to provide meaningful results for $\rho^* \geqslant 0.920$. In Fig. 5 the value of $\alpha_2(t^*)$ is plotted as a function of the reduced time for $0.860 \leqslant \rho^* \leqslant 0.920$. The value of $\alpha_2(t^*)$ exhibits a maximum whose magnitude increases as the density increases. The time for which $\alpha_2(t^*)$ is maximum $t^*_{\max}$ increases exponentially with the density. For $\rho^* \leqslant 0.850$ the amplitude of this maximum is small (not shown).

In addition, for all densities at very short times ($\sim t^* = 0.1$–0.4), we find another maximum in $\alpha_2(t^*)$ versus t^*. These small amplitude maxima are displayed in Fig. 6 using a suitably expanded scale. The densities in Fig. 6 correspond to liquid far from the liquidus ($\rho^*=0.780$), hexatic near the solidus ($\rho^*=0.890$), and solid far from the solidus ($\rho^* = 0.960$); their amplitudes are 1–2 orders of magnitude smaller than those of the maxima at longer times displayed in Fig. 5. The time decays associated with these non-Gaussian modes are short so that their effect on the value of the integral of $\alpha_2(t^*)$ is negligible. In contrast to the behavior of the large amplitude maximum of $\alpha_2(t^*)$ at longer time, the value of $\alpha_2(t^*)$ at the small amplitude maximum and the time at which this maximum is observed decrease with the density.

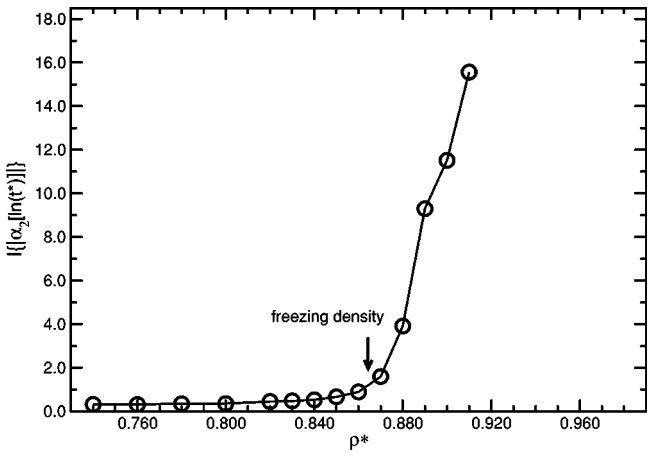

FIG. 4. The integral of the absolute value of the non-Gaussian parameter $|\alpha_2[\ln(t^*)]|$ over the natural logarithm of time, defined in Eq. (15), as a function of the two-dimensional number density.

In Fig. 7 the normalized velocity autocorrelation function is displayed. The time for which the function exhibits a minimum with a negative value (or a decay to zero) corresponds to the first collision; in a dense medium the first collision of an atom with its neighbors generates backscattering. The behavior shown in this figure is more pronounced at higher densities due to the cage effect, since the backscattering is more nearly parallel to the initial direction the higher the density, thereby generating a deeper minimum of the velocity autocorrelation function. The time at the minimum or at the decay to zero (when such a minimum is absent at low densities), corresponds to the time at which the small amplitude maximum of $\alpha_2(t^*)$, shown in Fig. 6, occurs. We infer that the deviation from Gaussian behavior at very short time (collision time) originates from the deviation from ballistic motion due to the first collision event. The shift of the location of the maximum to shorter times and the shift of the amplitude of the maximum to lower values as the density is increased is to be expected. At higher densities the collision time is shorter, which means that stochastic behavior is approached at shorter time and for smaller particle displacements, yielding smaller deviations of the particle displacement distribution from Gaussian form.

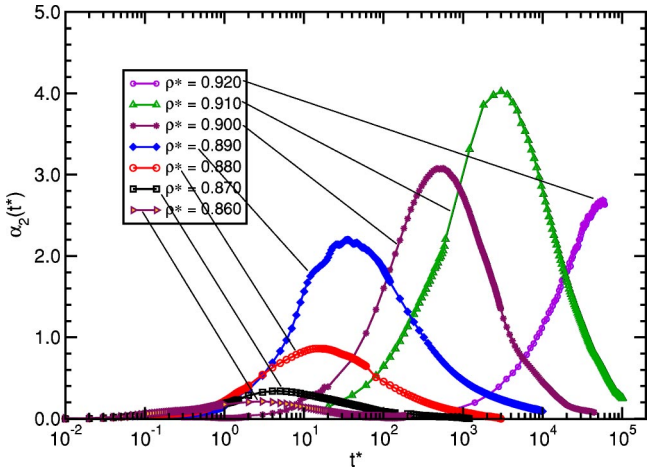

FIG. 5. (Color online) The non-Gaussian parameter $\alpha_2(t^*)$ as a function of the reduced time t^* for two-dimensional number densities $0.860 \leqslant \rho^* \leqslant 0.920$. The x axis is plotted on a logarithmic scale. The value of $\alpha_2(t^*)$ at the maximum as well as the time which the maximum appears increase for higher densities. The latter appears to depend exponentially on the density.

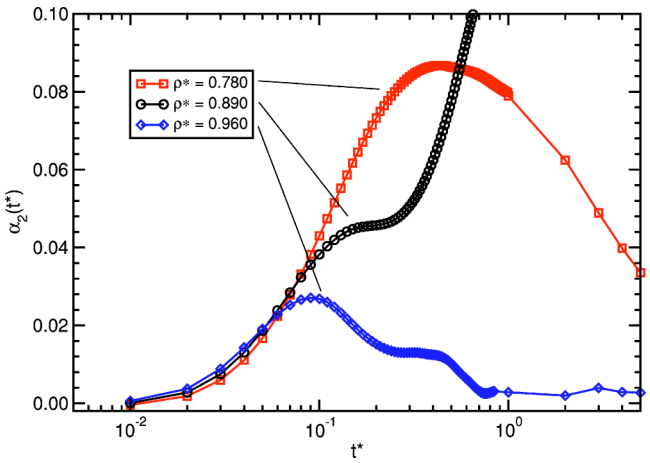

FIG. 6. (Color online) Magnification of $\alpha_2(t^*)$ at very short times $5\times10^{-3} \leqslant t^* \leqslant 5\times10^{0}$, for two-dimensional number densities that represent liquid far from freezing ($\rho^*=0.780$), hexatic near the melting point ($\rho^*=0.890$), and solid far from melting ($\rho^*=0.960$). The small-amplitude maximum of $\alpha_2(t^*)$, observed at very short times ($\sim t^*=0.1$–0.4), occurs for all densities. Note that in contrast to the behavior of the large-amplitude maximum of $\alpha_2(t^*)$ at longer time shown in Fig. 5, the value of $\alpha_2(t^*)$ at the maximum and the time at the maximum decrease with the density.

The time for which the large amplitude maximum of $\alpha_2(t^*)$ is observed (Fig. 5) encompasses many collision events. For example, the maximum for $\rho^*=0.890$ occurs at around $t^*_{\max}=35$. Given the information in Fig. 7 this corre-

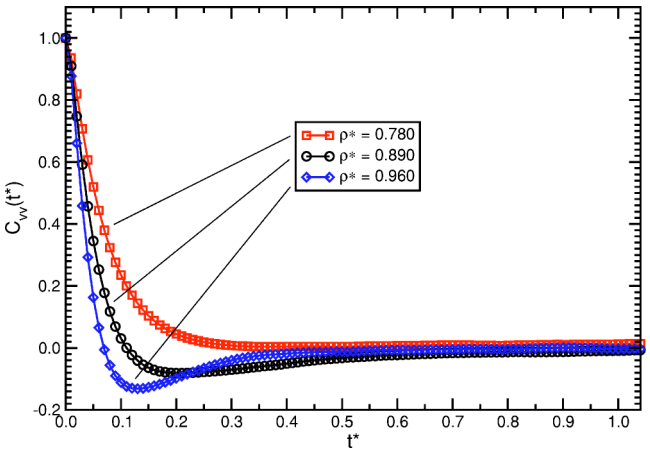

FIG. 7. (Color online) The normalized velocity autocorrelation function as a function of the reduced time for the three densities shown in Fig. 6. The velocities are calculated only for the lateral components in the xy plane. The time for which the function exhibits a minimum (or a decay to zero) is the time it takes the particles to travel between collisions and it corresponds to the time for which the small-amplitude maximum of $\alpha_2(t^*)$ shown in Fig. 6 is observed.

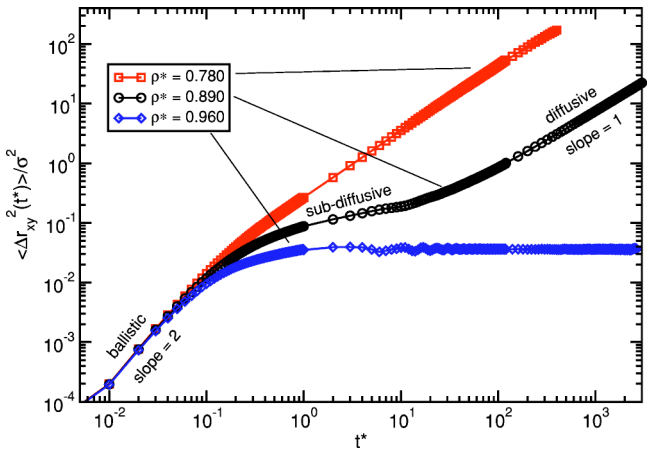

FIG. 8. (Color online) The lateral mean squared displacement (in reduced units) as a function of the reduced time for the three densities shown in Figs. 6 and 7. Both axes are plotted on a logarithmic scale. For $\rho^*=0.890$ the plot exhibits three different dynamic relaxations modes. The onset of the relaxation mode at long time corresponds to the location of the maximum of $\alpha_2(t^*)(\sim t^*=35)$ shown in Fig. 5.

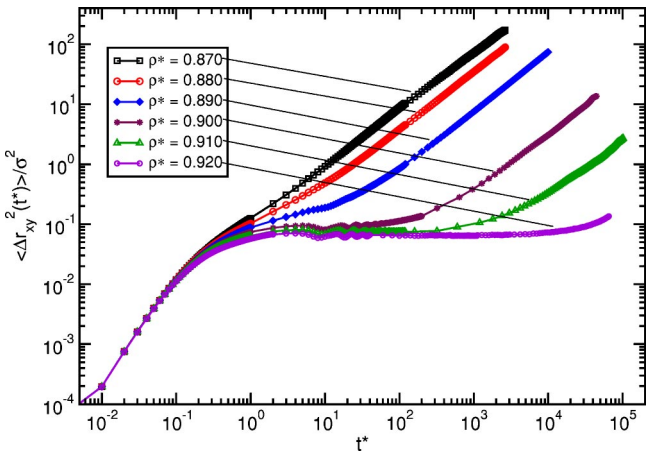

FIG. 9. (Color online) The lateral mean squared displacement (in reduced units) as a function of the reduced time for two-dimensional number densities $0.860\leqslant\rho^*\leqslant0.920$. The curves show the emergence of the three dynamic relaxation modes. The slope of the mean squared displacement for the longest relaxation mode is linear for all densities indicating diffusive behavior. However, the slope for the intermediate relaxation mode is sublinear for densities lower, and vanishes for densities higher, than the melting density. The time of the onset of the longest relaxation mode increases exponentially with the density and it corresponds to the time for which $\alpha_2(t^*)$ is maximum.

sponds to 180 collision times. For $\rho^*=0.910$ the maximum of $\alpha_2(t^*)$ is observed at $t^*_{\max}=3000$. This corresponds to 1.7×10^4 collision times. It appears that $t^*_{\max}$ increases exponentially with the density.

In Fig. 8 we display the lateral mean squared single particle displacement as a function of the reduced time for the two-dimensional number densities shown in Figs. 6 and 7. For t^* shorter than the particle collision time ($t^*\leqslant0.1$) the plots for all densities overlap as expected for density independent ballistic motion. At long times, the particle motion for the liquid far from freezing ($\rho^*=0.780$) is diffusive, i.e., the mean squared displacement is a linear function of time. For the solid far from the solidus ($\rho^*=0.960$) the dynamics at times as long as they were reached during the current simulations can be described as vibrations around lattice points; then the mean squared displacement is a constant. For the hexatic phase near the solidus ($\rho^*=0.890$), three distinct regions of the mean squared displacements can be identified. At times longer than the collision time but shorter than the long time behavior (''intermediate time''), the dependence of the mean squared displacement on time is sublinear. At long time, the motion is diffusive, as is indicated by the linear slope, the same as that observed for the liquid far from freezing ($\rho^*=0.780$). Note that for $\rho^*=0.890$ the onset of the long-time dynamical relaxation mode is the same as $t^*_{\max}$ identified in Fig. 5.

Figure 9 displays the mean squared displacement for the density range $0.870\leqslant\rho^*\leqslant0.920$, showing the emergence of the three dynamical relaxation processes. The intermediate relaxation time appears for $\rho^*\geqslant0.870$ and is broadened as the density increases. This region, with a sublinear slope for densities between the liquidus and the solidus, attains a zero slope when the system becomes completely solid ($\rho^*=0.900$). The results indicate that the slowing down in the particle motion at intermediate times originates from the cage effect. The onset of long-time dynamics increases exponentially with the density and it corresponds to the time for which $\alpha_2(t^*)$ is maximum. The slope at intermediate times observed for $\rho^*=0.870$–0.890 is greater than zero but smaller than one, which is a consequence of dynamical heterogeneity (Fig. 10); there are two-dimensional ''ordered''

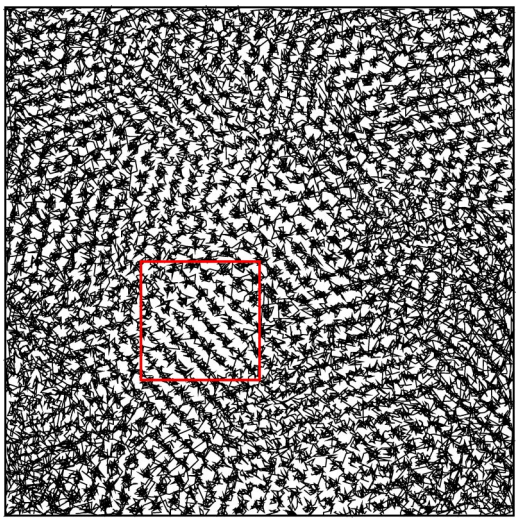

FIG. 10. (Color online) A section of the simulation box (length of box vector is 30σ in each direction) for $\rho^*=0.880$ showing the particle trajectories. The total number of frames is 41 separated by time interval $\Delta t^*=2.5$, so that the duration of each trajectory is $t^*=100$. At this density, $t^*_{\max}=16$ and $\langle\Delta r^2_{xy}(t^*=100)\rangle=3.78$. The heterogeneity of the particle motion is evident, as are the vibrational modes and correlated diffusion along the directions with strong bond orientation correlation. The region indicated by the square is plotted in Fig. 11.

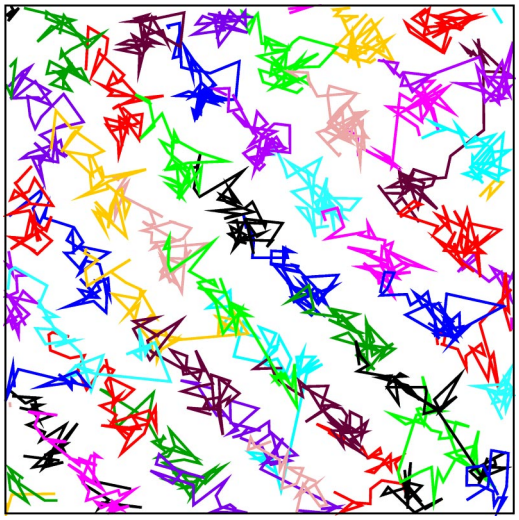

FIG. 11. (Color) The same trajectory displayed in Fig. 10, shown on a smaller scale (length of box vector is 7σ in each direction) and for an ordered domain. Trajectories of different particles are depicted in different colors.

domains (contributing zero to the slope of the mean squared displacement) and one-dimensional ''disordered'' domains (occurring at the boundaries of the ''ordered'' domains). The resulting displacement dynamics, therefore, has a mixed character. The coexistence between the dynamically ordered and disordered domains occurs for densities inside the plateau region of the lateral pressure-density isotherm even though our simulation results do not display clear coexistence between liquid and hexatic and hexatic and solid phases. The motion of the particles in the ''disordered'' domain during $t^*_{\max}$ is cooperative and quasi-one-dimensional (stringlike), yielding the observed deviation from Gaussian form of the displacement distribution.

Figure 10 shows the trajectory of the particles for a section of the simulation box for $\rho^*=0.880$. The time covered is in the range $0 \leqslant t^* \leqslant 100$, which is about $6t^*_{\max}$. For this density and for this time interval the mean squared displacement $\langle \Delta r^2_{xy}(t^*=100)\rangle = 3.78$. Thus, the trajectories of most of the particles in this figure represent diffusion for a distance of about 2 particle diameters. The cooperative motion of the particles can be seen clearly in Fig. 11 where the attention is focused on an ordered domain and different particle trajectories are depicted in different colors. It is clear the system is dynamically heterogeneous and that the diffusive paths of the particles are along the directions with strong bond orientation correlation.

It is computationally very demanding to approach the long time scale for $\rho^* \geqslant 0.920$, therefore we are unable get meaningful dynamical results for this region of the solid phase. Our analysis at short and intermediate time scales reveals very small values of the integral of $\alpha_2(t^*)$ (plotted in Fig. 4) and mean squared displacements independent of the time, the same as plotted in Fig. 8 for $\rho^*=0.960$. Thus, for short and intermediate times the particle displacement distribution of this system has a Gaussian form.

The time-dependent distributions of the particles motion

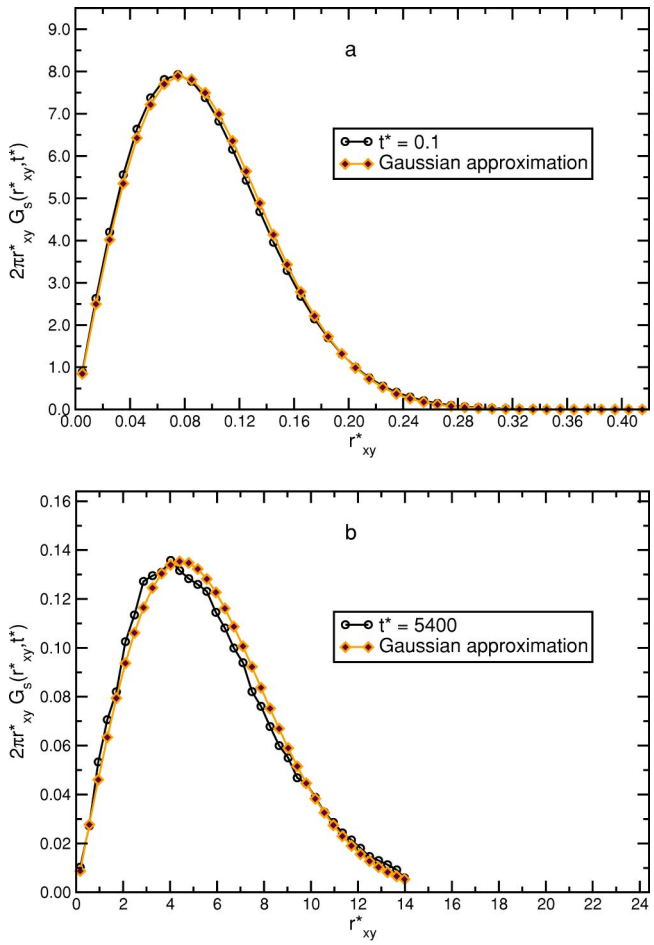

FIG. 12. (Color online) The self-part of the van Hove function, multiplied by the radial element $2\pi r_{xy}$, as a function of the reduced lateral interparticle distance, plotted for $\rho^*=0.890$ at (a) short time ($t^*=0.1$) and (b) long time ($t^*=5400$). The function describing the single particle distribution derived from the Gaussian approximation [Eq. (1)] is also plotted. The values of the mean squared displacement $\langle \Delta r^2_{xy}(t^*=0.1)\rangle = 0.0118$ and $\langle \Delta r^2_{xy}(t^*=5400)\rangle = 40.14$, were taken from Fig. 8.

were analyzed using the van Hove functions. In Fig. 12 we plot the self-part of the van Hove function at short ($t^*=0.1$) and long ($t^*=5400$) times for $\rho^*=0.890$. We also plot the function $[2r_{xy}/\langle \Delta r^2_{xy}(t)\rangle]e^{-r^2_{xy}/\langle \Delta r^2_{xy}(t)\rangle}$, which is the expression for $G_s(r_{xy},t)$ obtained from the Gaussian approximation [Eq. (1)] multiplied by the radial element $2\pi r_{xy}$. The values of $\langle \Delta r^2_{xy}(t)\rangle$ were taken from independent simulations results shown in Fig. 8, namely, $\langle \Delta r^2_{xy}(t^*=0.1)\rangle = 0.0118$ and $\langle \Delta r^2_{xy}(t^*=5400)\rangle = 40.14$. Hence, there are no fitted parameters for the Gaussian form. The figures show that for the short and long time regimes the Gaussian approximation is almost identical to the simulation results. Note that $G_s(r_{xy},t)$ is multiplied by $2\pi r_{xy}$ to cancel the radial averaging that is introduced in Eq. (17). This is necessary because the single-particle displacement distribution at intermediate times is not radially homogeneous; it is essentially that resulting from motion in one dimension. Figure 13 displays the distinct part of the van Hove function for the short and long times analyzed in Fig. 12. At short time,

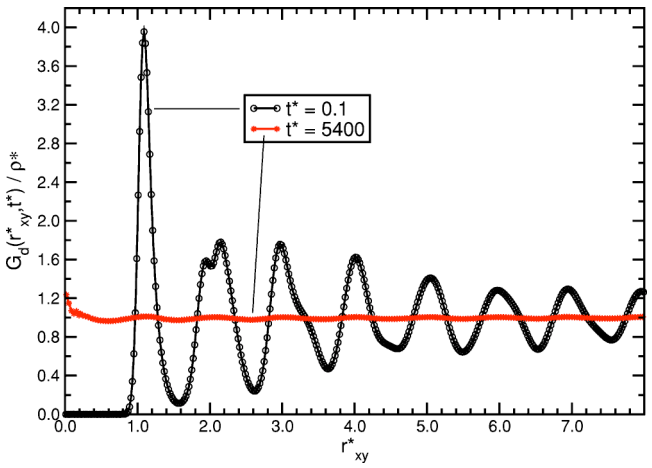

FIG. 13. (Color online) The distinct-part of the van Hove function, normalized by the reduced two-dimensional number density, as a function of the reduced lateral interparticle distance, plotted for $\rho^*=0.890$ at the short and the long times analyzed in Fig. 12. The short time behavior of $G_d(r_{xy},t)$ exhibits structure that is similar to the static pair distribution function $g(r)$. On the other hand, the long time behavior of $G_d(r_{xy},t)$ is constant.

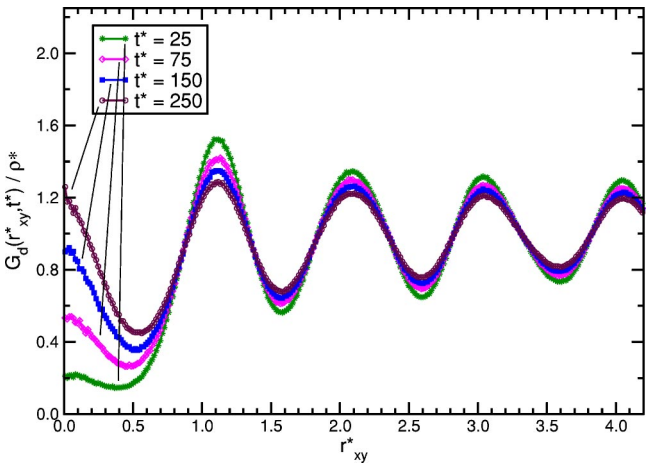

FIG. 15. (Color online) The distinct-part of the van Hove function, normalized by the reduced two-dimensional number density, as a function of the reduced lateral interparticle distance, plotted for $\rho^*=0.890$ at the times analyzed in Fig. 14. For the times shown, the increase of $G_d(r_{xy},t)/\rho^*$ at $r_{xy}=0.0$ with time, and the minimum of $G_d(r_{xy},t)/\rho^*$ at $r_{xy}=0.5$, points to the discontinuity of the particle motion.

$G_d(r_{xy},t)$ is very similar to $g(r_{xy})$. At long time, $G_d(r_{xy},t)$ is sensibly independent of r_{xy} as expected from stochastic particle dynamics.

In contrast to the behavior at short and long times, the particle dynamics at the transition from intermediate time to long time is very different. As shown above, there is a correlation between the location of $t_{\max}$ and the time for which the diffusive behavior begins. Figure 14 exhibits the self-part of the van Hove function for four times around $t^*_{\max}$ (for $\rho^*=0.890$, $t^*_{\max}\sim 35$). The curves exhibit multiple maxima

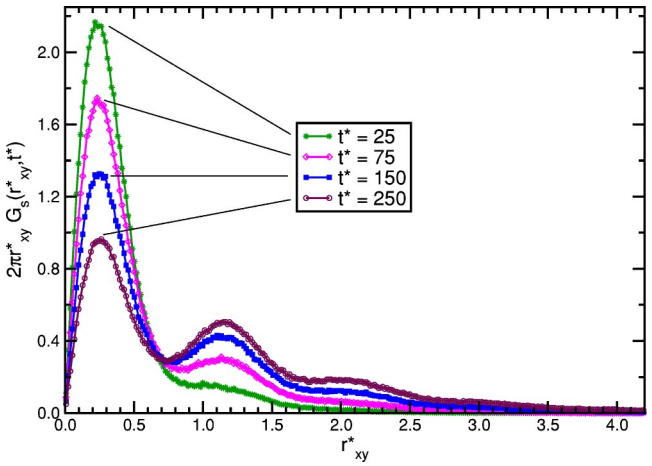

FIG. 14. (Color online) The self-part of the van Hove function, multiplied by the radial element $2\pi r_{xy}$, as a function of the reduced lateral interparticle distance, plotted for $\rho^*=0.890$ at four values of time around $t^*_{\max}\sim 35$. The multiple maxima observed, as the time increases, separated by a distance corresponding to the particle diameter indicate dynamical heterogeneity and that the motion of the particles are described by correlated ''jumps'' to a neighboring site and not via continuous diffusion.

indicating that the dynamics is heterogenous and that the particles experience cooperative ''jumps'' from one site to another. Thus, at specific values of time there are different subsets of particles that travel for different distances. The fact that these maxima are separated by a distance that corresponds the particle diameter indicates that the jump dynamics, over 2–3 particle diameters, is in one dimension. Figure 15 displays the distinct part of the van Hove function for the same times as in Fig. 14. It is evident that as t^* increases from 25 to 250 the probability of finding a particle at the location where another particle resided at $t^*=0$ increases dramatically. The minimum of the probability distribution at $r^*_{xy}=0.5$ confirms the picture of ''jumps'' rather than continuous diffusion.

Correlated jump dynamics also occurs in the solid phase. Figure 16 displays the self-part of the van Hove function for $\rho^*=0.910$ at times in the range $2500\leqslant t^*\leqslant 140\,000$. The curves are similar to those shown in Fig. 14. However, the number of maxima is larger and they are better resolved, which indicates greater heterogeneity and stronger dynamical correlations. The amplitude of the first peak decreases with time so that for $t^*\geqslant 98\,000$, the second peak of $G_s(r_{xy},t)$ has a larger amplitude than the first peak, which indicates that the majority of the particles have already diffused at least one lattice site. Figure 17 displays the corresponding distinct part of the van Hove function; it shows a large increase at $r_{xy}=0.0$ as the time increases while for larger values of r_{xy} it is hardly changed.

As is shown in Fig. 9, at very long time the colloid particle motion for all densities, even for densities in the solid phase, is diffusive. Cooperative jumps that lead to a diffusive process in crystals can be explained by a mechanism that involves many such correlated hops in random locations and random directions (along the crystallographic axes) yielding random walk behavior.

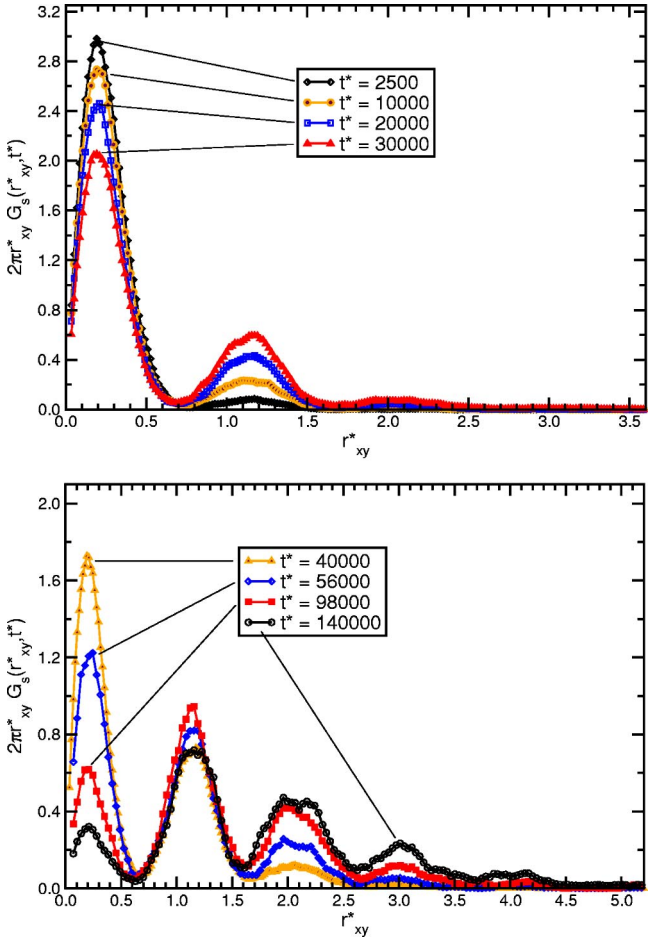

FIG. 16. (Color online) Same as Fig. 14 but for a density that corresponds to the solid phase $\rho^*=0.910$. Note that the amplitude of the first peak decreases while the number of peaks increase with time. $G_s(r_{xy},t)$ at $t^*=140\,000$ exhibits five maxima.

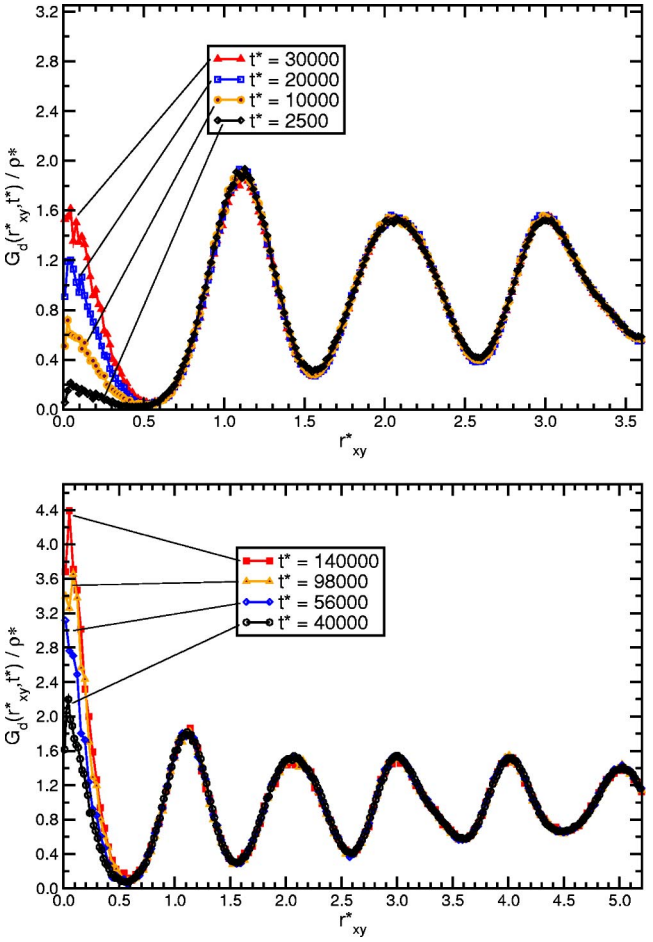

FIG. 17. (Color online) Same as Fig. 15 but for a density that corresponds to the solid phase $\rho^*=0.910$. $G_d(r_{xy},t)$ exhibits a large increase at $r_{xy}=0.0$ as the time increases while for larger values of r_{xy} it does not change.

The amplitude of $\alpha_2(t^*)$ is small in the liquid phase and a third (intermediate) dynamical relaxation process is not observed. However, the particle trajectories are heterogenous and the corresponding displacement distribution is non-Gaussian. This can be seen in Fig. 18 where we display the particle trajectories for a density in the liquid phase $\rho^*=0.820$ for a time period of $t^*=6$. At this density, $t^*_{\max}=1.2$ and $\langle \Delta r^2_{xy}(t^*=6)\rangle = 1.41$. The cooperativity of the particle motion is evident in linear stringlike paths and in circular paths with an immobile particle in the center.

The results of this study and of computational and experimental studies of other systems imply that the deviation of the distribution of particle displacements from Gaussian form is universal. Although our results are for a system with a colloid-colloid potential that is everywhere repulsive, very similar results have been obtained for systems with the Marcus-Rice and modified Marcus-Rice potentials that were designed to represent colloidal particles that are sterically stabilized with grafted polymers [45,48]. It is worth noting that the change in the colloid-colloid interaction does cause a marked change in the thermodynamic behavior of the system in the high-density region of the phase diagram [50].

IV. DISCUSSION

The results presented in this paper reveal a strong correlation between the dynamical and the thermodynamic behavior of a quasi-two-dimensional system. Although dynamical heterogeneity and correlated motion are present in the liquid phase, at the liquidus the distribution of single-particle displacements develops a strong deviation from Gaussian form and the mean squared displacement as a function of time exhibits a third relaxation region at intermediate times that is characterized by a sublinear slope. The onset of this behavior is associated with the transition from the liquid to a hexatic phase with long-ranged bond orientation order. At the solidus this sublinear slope becomes zero for intermediate time.

The deviation of the single-particle displacement distribution from Gaussian form is a result of correlated motion that has also been observed in real quasi-two-dimensional colloid suspensions. The results that are presented here show that the correlated motion becomes relatively more important in the solid phase. The continuous behavior of this mode of motion from the liquid phase through the hexatic phase and into the crystalline phase suggests that it arises from the same physical phenomenon. It is logical to assign the driver for motion

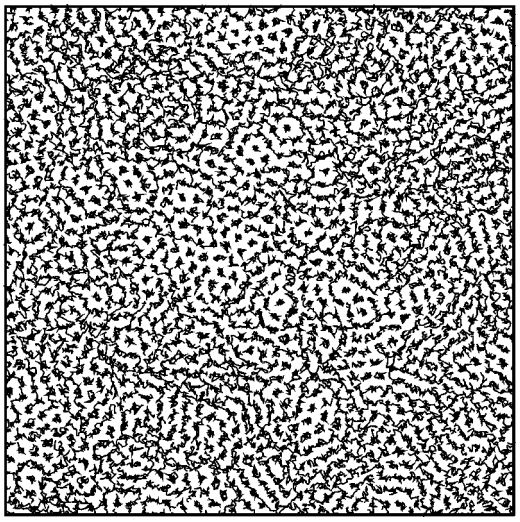

FIG. 18. A section of the simulation box (length of box vector is 40σ in each direction) displaying the particle trajectories for a density in the liquid phase $\rho^*=0.820$. The total number of frames is 41 separated by time interval $\Delta t^*=0.15$, so that the duration of each trajectory is $t^*=6$. At this density, $t^*_{\max}=1.2$ and $\langle \Delta r^2_{xy}(t^*=1.2)\rangle = 0.249$. The cooperativity of the particle motion is present as linear and circular strings of motion.

in the solid phase to superpositions of normal mode vibrations along paths that generate activated hopping of a particle. Normal mode analysis of the motion of a many-body system is rigorously possible in crystals for which the restoring forces acting on a particle are linear in the displacement of the particle from its equilibrium position [51]. Nevertheless, Zwanzig has argued that collective variables, analogous to longitudinal and transverse phonons in crystals, do exist in classical liquids [52]. He noted, however, that their lifetimes are exceedingly short except in the glassy state. This idea has been followed up by Stratt and co-workers [53,54] and Keyes and co-workers [55,56] via the definition of instantaneous normal modes of a liquid.

The fact that the appearance of the cooperative modes starts at the density at which the hexatic phase starts to appear points to the dependency of the existence of the normal modes on a medium with a critical degree of bond orientation correlation. We suggest that the correlated motion, even at densities lower than the solidus density, is a result of superposition of instantaneous normal mode excitations with a free energy greater than the free energy barrier for hopping. As the density increases, the life times of the instantaneous normal vibrations increase, thereby allowing more effective competition between cooperative hopping motion and independent particle motion, so that the cooperative hopping becomes increasingly dominant as the density increases. The natural hopping directions are along axes with strong bond orientation correlation.

From a free energy landscape point of view, the slowing down in the dynamics at intermediate times can be interpreted in terms of trapping in local minima. Then the transitions from one local minimum to another define the displacement dynamics of the system. This picture was first introduced by Goldstein with respect to the glass transition [57]. In a recent development with the same conceptual basis, Halpern extended the random energy model for three-dimensional supercooled liquids to include two routes for the particles to leave their traps by thermal excitation. The correlated motion of a group of particles was assigned a lower activation energy and a smaller prefactor (a smaller matrix element for the transition) than independent particle motion, so that at low temperature it dominates the diffusion mechanism [58].

There is a striking similarity between the distribution of single-particle displacements in a quasi-two-dimensional liquid near the liquidus with that obtained near the glass transition for glass forming liquids. However, there is also a fundamental difference between these results. The glass transition is a kinetic effect in the sense that it does not correspond to the global minimum of the free energy of the system, hence the particle motion near the glass transition will tend to drive the system towards a more stable state. On the other hand, the correlated motion in a quasi-two-dimensional liquid is present in the field of equilibrium states of the system and both the structural and thermal properties of the system are independent of the time.

ACKNOWLEDGMENTS

The research reported in this paper was supported by the European Community, the Fifth Framework Program, under Contract No. MCFI-1999-00161 and by the National Science Foundation via Grant No. NSF-CHE 9977841.

[1] J.P. Hansen and I.R. McDonald, *Theory of Simple Liquids*, 2nd ed. (Academic Press, London, UK, 1986).
[2] B.R.A. Nijboer and A. Rahman, Physica (Amsterdam) **32**, 415 (1966).
[3] A. Rahman, Phys. Rev. **136**, A405 (1964).
[4] D. Levesque and L. Verlet, Phys. Rev. A **2**, 2514 (1970).
[5] W. Kob, C. Donati, S.J. Plimpton, P.H. Poole, and S.C. Glotzer, Phys. Rev. Lett. **79**, 2827 (1997).
[6] C. Donati *et al.*, Phys. Rev. Lett. **80**, 2338 (1998).
[7] W.K. Kegel and A. van Blaaderen, Science **287**, 290 (2000).
[8] E.R. Weeks, J.C. Crocker, A.C. Levitt, A. Schofield, and D.A. Weitz, Science **287**, 627 (2000).
[9] M.M. Hurley and P. Harrowell, Phys. Rev. E **52**, 1694 (1995).
[10] M.M. Hurley and P. Harrowell, J. Chem. Phys. **105**, 10521 (1996).
[11] D.N. Perera and P. Harrowell, J. Chem. Phys. **111**, 5441 (1999).
[12] C. Reichhardt and C.J.O. Reichhardt, Phys. Rev. Lett. **90**, 095504 (2003).
[13] A.H. Marcus, J. Schofield, and S.A. Rice, Phys. Rev. E **60**, 5727 (1999).
[14] B. Cui, B. Lin, and S.A. Rice, J. Chem. Phys. **114**, 9142

(2001).
[15] G. Adam and J.H. Gibbs, J. Chem. Phys. **43**, 139 (1965).
[16] M.T. Cicerone and M.D. Ediger, J. Chem. Phys. **103**, 5684 (1995).
[17] B. Doliwa and A. Heuer, Phys. Rev. Lett. **80**, 4915 (1998).
[18] D. Caprion, J. Matsui, and H.R. Schober, Phys. Rev. Lett. **85**, 4293 (2000).
[19] T.B. Schrøder, S. Sastry, J.C. Dyre, and S.C. Glotzer, J. Chem. Phys. **112**, 9834 (2000).
[20] A. Heuer and K. Okun, J. Chem. Phys. **106**, 6176 (1997).
[21] C. Bennemann, C. Donati, J. Baschnagel, and S.C. Glotzer, Nature (London) **399**, 246 (1999).
[22] Y. Gebremichael, T.B. Schroder, F.W. Starr, and S.C. Glotzer, Phys. Rev. E **64**, 051503 (2001).
[23] E. Leutheusser, Phys. Rev. A **29**, 2765 (1984).
[24] U. Bengtzelius, W. Götze, and A. Sjölander, J. Phys. C **17**, 5915 (1984).
[25] W. Götze and L. Sjögren, Rep. Prog. Phys. **55**, 241 (1992).
[26] J. Schofield, A.H. Marcus, and S.A. Rice, J. Phys. Chem. **100**, 18950 (1996).
[27] *Diffusion*, edited by H. I. Aaronson (American Society for Metals, Metals Parks, OH, 1986).
[28] S.A. Rice, Phys. Rev. **112**, 804 (1958).
[29] S.A. Rice and N.H. Nachtrieb, J. Chem. Phys. **31**, 135 (1959).
[30] O.P. Manley and S.A. Rice, Phys. Rev. **117**, 632 (1960).
[31] A.W. Lawson, S.A. Rice, R.D. Corneliussen, and N.H. Nachtrieb, J. Chem. Phys. **32**, 447 (1960).
[32] S.A. Rice and H.L. Frisch, J. Chem. Phys. **32**, 1026 (1960).
[33] F. Bloch, Z. Phys. **61**, 206 (1930).
[34] R. Peierls, *Surprises in Theoretical Physics* (Princeton University Press, Princeton, 1979).
[35] N.D. Mermin, Phys. Rev. **176**, 250 (1968).
[36] L. Landau and E. Lifshitz, *Statistical Physics* (Pergamon Press, Oxford, 1986).
[37] J.M. Kosterlitz and D.J. Thouless, J. Phys. C **5**, L124 (1972).
[38] J.M. Kosterlitz and D.J. Thouless, J. Phys. C **6**, 1181 (1973).
[39] B.I. Halperin and D.R. Nelson, Phys. Rev. Lett. **41**, 121 (1978).
[40] D.R. Nelson and B.I. Halperin, Phys. Rev. B **19**, 2457 (1979).
[41] A.P. Young, Phys. Rev. B **19**, 1855 (1979).
[42] A. Zippelius, Phys. Rev. A **22**, 732 (1980).
[43] L. Verlet, Phys. Rev. **159**, 98 (1967).
[44] W.C. Swope, H.C. Andersen, P.H. Berens, and K.R. Wilson, J. Chem. Phys. **76**, 637 (1982).
[45] R. Zangi and S.A. Rice, Phys. Rev. E **58**, 7529 (1998).
[46] F.P. Preparata and M.I. Shamos, *Computational Geometry, An Introduction* (Springer-Verlag, New York, 1985).
[47] L. van Hove, Phys. Rev. **95**, 249 (1954).
[48] A.H. Marcus and S.A. Rice, Phys. Rev. E **55**, 637 (1997).
[49] P. Karnchanaphanurach, B. Lin, and S.A. Rice, Phys. Rev. E **61**, 4036 (2000).
[50] R. Zangi and S.A. Rice, Phys. Rev. E **61**, 671 (2000).
[51] M. Born and K. Huang, *The Dynamical Theory of Crystals* (Oxford University Press, Oxford, 1955).
[52] R. Zwanzig, Phys. Rev. **156**, 190 (1967).
[53] M. Buchner, B.M. Ladanyi, and R.M. Stratt, J. Chem. Phys. **97**, 8522 (1992).
[54] R.M. Stratt, Acc. Chem. Res. **28**, 201 (1995).
[55] T. Keyes, J. Chem. Phys. **101**, 5081 (1994).
[56] T. Keyes, J. Phys. Chem. A **101**, 2921 (1997).
[57] M. Goldstein, J. Chem. Phys. **51**, 3728 (1969).
[58] V. Halpern, Philos. Mag. B **81**, 1237 (2001).